Newcastle University

School of Mathematics & Statistics

MMath Project

Modelling Magnetic Activity in the Sun

Author:
Joshua Kirk

Supervisor:
Dr. Paul J. Bushby

Abstract

The Sun exhibits a large-scale oscillatory magnetic field which is sustained by dynamo action. In this project, we study the effects of a parameterized nonlinear η-quenching term in a 1D Cartesian model of the solar dynamo. This model also includes other quenching mechanisms which will be described in this report. By exploring parameter space with different initial conditions, we find overlapping solution branches, and by increasing the strength of the η-quenching parameter we show that these regions of bistability can grow.

Contents

1 Observations of the solar magnetic field

1.1 Introduction

There is a wide consensus that the generation of the Sun's magnetic fields is due to dynamo action. The underlying processes of the dynamo, and origins of the magnetic field, remain topics of great interest, of which modelling is a vital part of research and development. Solar dynamo theory is not only a subject that is studied solely for academic interest, the magnetic fields of the Sun have far reaching consequences here on Earth: influencing climate, protecting us from cosmic radiation and affecting our satellite navigation systems. This introduction will be split into two sections, first there is a brief introduction of how observations of the Sun gives evidence for magnetic fields, followed by a description of the interior structure of the Sun. The second part of the introduction discusses an overview of basic dynamo theory, including equations, relevant physical mechanisms and problems that arise.

1.2 Sunspots

A spectacular feature of the Sun is its sunspots (See figure 1); dark areas that appear on the solar surface which are now known to be the surface manifestation of a strong azimuthal magnetic field (Tobias, 2002), this magnetic field is also called a '*toroidal magnetic field*', (Parker, 1955).

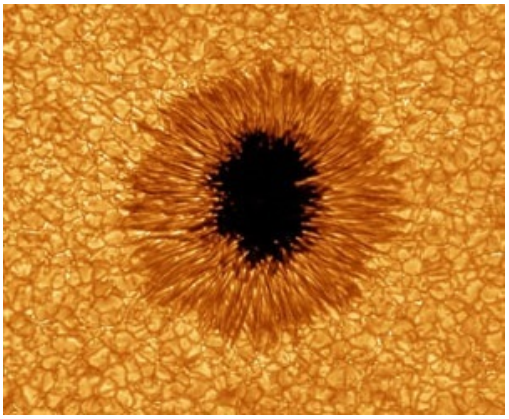

Figure 1: A Sunspot: The dark patch is cooler in temperature than its surroundings[I]

By observing the behaviour of sunspots we can infer the properties of the underlying azimuthal component of the magnetic field that is the toroidal magnetic field. The toroidal magnetic field lies deep in the interior of the solar structure, and sunspots are a consequence of toroidal flux ropes that rise to the surface due to magnetic buoyancy. For more details, see Parker (1955).

Observations of sunspots over time have shown that the average number of spots on the surface varies cyclically, with a mean

[I]Figure 1 source: `http://newswatch.nationalgeographic.com/files/2010/09/sunspot-closeup-nasa.jpg`

period of 11 years. This is called the solar cycle. The sunspots not only vary in number, but vary in latitude, with spots forming at latitudes of ±30°at the beginning of each cycle. Zones of sunspot formation move towards to the Sun's equator as the cycle progresses. This connection between cyclic and latitudinal behaviour, known as Spörer's law (Babcock, 1961), produces the famous butterfly diagram (see figure 2).

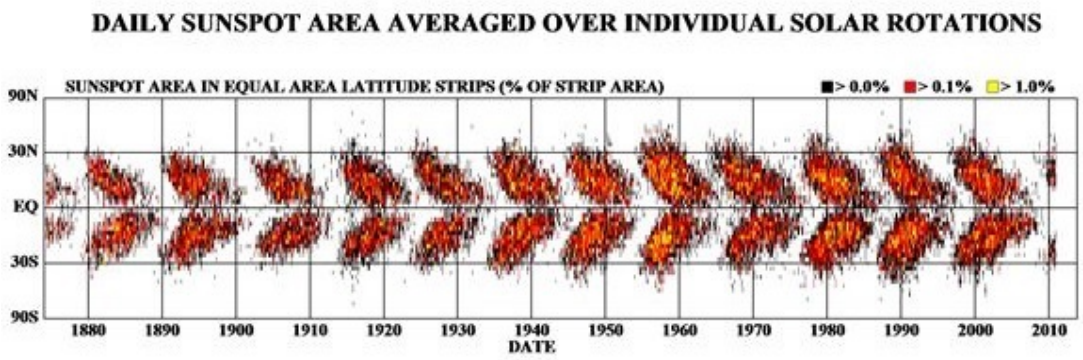

Figure 2: The butterfly diagram[II]

Sunspots appear in pairs with opposite magnetic polarities, which swap polarity at the end of each 11 year cycle (Cowling, 1935). Therefore the full '*magnetic cycle*' has a mean period of 22 years. The larger pairs sometimes appear with a tilt towards the east-west direction. The leading sunspot is closer to the solar equator than the trailing spot, (this is known as Joy's Law (Hale et al., 1919)).

In conjunction with these 11 year cycles there is also modulation on longer timescales. This can lead to a lack of sunspots for an extended period of time. These grand minima have a mean period of approximately 200 years, the last grand minima (the "Maunder Minimum") started in the 17th century stretching from 1645 to 1715. In those 70 years there were few sunspots seen on the solar surface, and this was later noticed by G.Spörer and E.W. Maunder (Eddy, 1976). During this period the magnetic field still

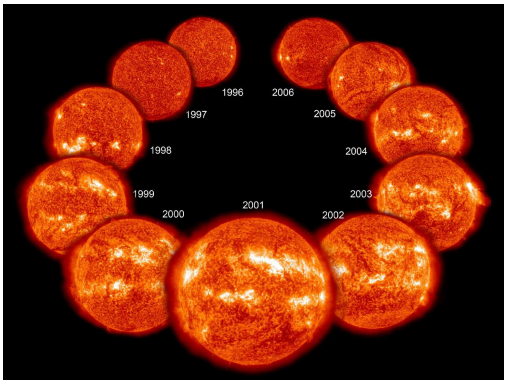

Figure 3: Surface activity over 10 yearrs between 1996 and 2006[III]

[II]Figure 2 source: `http://www.nasa.gov/images/content/144051main_ButterflyDiagramLG.jpg`

[III]Figure 3 source: `http://www.nasa.gov/images/content/524990main_FAQ10_full.jpg`

oscillated, although at a much lower amplitude. At the end of the Maunder Minimum, sunspots only appeared in the southern hemisphere before returning to either side of the equator after one asymmetric cycle. The analysis of ^{10}Be in polar icecaps or ^{14}C in tree rings can give grand minima records over the past 4000 years.

1.3 Coronal field

Besides sunspots, there is also the solar corona which is evidence of the radial component of the magnetic field. This radial component is called the '*poloidal magnetic field*', and alternates out of phase with the toroidal field (Stix, 1976). So at a sunspot maximum, the poloidal field is at a minimum and reverses.

The coronal field is most prominent during solar eclipses and has much higher temperatures than the Sun's surface, with temperatures around several million Kelvin compared to the photosphere (which has a temperature of approximately 6000K). This is another solar physics problem in its own right, which has links with the magnetic field. However although an interesting curiosity, it is not part of this report, but an example of why the solar dynamo problem is such a hot topic (literally) for its scope of problems.

These observations are sufficient evidence for the solar magnetic fields, how these fields are generated and interact with each other is part of the dynamo problem. In order to develop the concept of the dynamo problem, we need to know the interior structure of the Sun and how this leads to the possibility that there is magnetic field generation within the solar interior.

1.4 Internal structure

The Sun's interior structure consists of a solid core at the centre, a rapidly rotating radiative zone that stretches to approximately 70% of the radius, and (more importantly for dynamo action) it is followed by a differentially rotating, highly turbulent plasma containing many eddies on a wide range of spatial and temporal scales. The outer 30% of the Sun's interior is called the convection zone. This convection zone includes the photosphere in which small scale convection manifests itself on the surface in the form of granulation (Stix, 2004).

The relative motion of sunspots at different latitudes first led to the conclusion that the Sun rotates differentially, and the science of helioseismology can give more information on how this convection zone rotates at varying latitudes and depths. This differential rotation is key to dynamo action, as differential shearing

is responsible for the process of converting the poloidal field to a toroidal field. The greatest shear is found in a thin layer between the radiative and convection zones called the tachocline (see figure 4) and is believed to be the location of the solar dynamo (J.Mason et al., 2002).

The tachocline can also store magnetic fields for a substantial length of time (Tobias, 2002). As the magnetic field is stored it is wound up by the differential rotation and increases in strength. Eventually, the field becomes strong enough such that it becomes unstable to magnetic buoyancy instabilities which, as mentioned earlier, leads to the formation of sunspots.

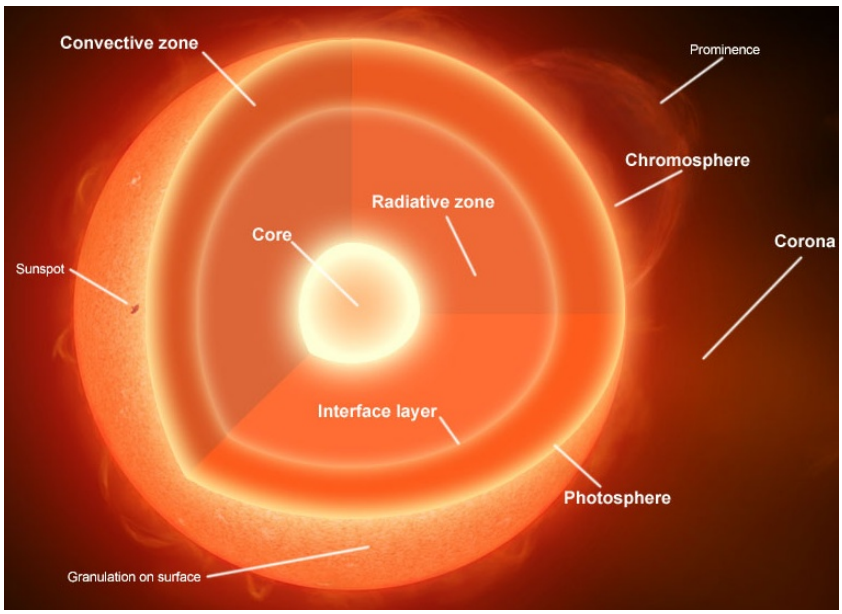

Figure 4: The Tachocline (interface layer) is located between the convective and radiative zones[IV]

2 Dynamo theory

The dynamo problem is finding a flow field that has inductive properties capable of sustaining a magnetic field against ohmic dissipation (Charbonneau, 2010). Ohmic dissipation describes the loss of electric energy when a current flows through a conducting medium, leading to the production of heat (McGraw-Hill, 2003).

[IV] Figure 4 source: `http://astronomy.nmsu.edu/msussman/tachocline/basic1.html`

2.1 Magnetic induction

Since the convection zone in the solar interior is a magnetized plasma, we should consider Maxwell's equations, Ohm's law (for a moving conductor, as we have a flow) and Ampère's law. Maxwell's equations are,

$$\nabla \cdot \mathbf{E} = \frac{\rho_e}{\epsilon_0}, \tag{1}$$

$$\nabla \cdot \mathbf{B} = 0, \tag{2}$$

$$\nabla \times \mathbf{E} = -\frac{\partial \mathbf{B}}{\partial t}, \tag{3}$$

$$\nabla \times \mathbf{B} = \mu_0 \mathbf{j}, \tag{4}$$

where $\mathbf{B}$ is the magnetic field, $\mathbf{E}$ is the electric field, ρ_e is the charge density, c is the speed of light, ϵ_0 is permitivity, μ_0 is the magnetic constant and $\mathbf{j}$ is the current density. Ohm's law for a moving conductor is,

$$\mathbf{j} = \sigma(\mathbf{E} + \mathbf{u} \times \mathbf{B}), \tag{5}$$

where σ is the electrical conductivity. There is an added effect of current that is induced by the Lorentz force, due to the fluid moving, which is the $\mathbf{u} \times \mathbf{B}$ term (in the rest frame $\mathbf{u} = 0$ so this additional term would not contribute).

In order to actually solve the dynamo problem, the solution to the evolution equation of the magnetic field and the equation describing the motion of the fluid should be found. The evolution equation of the magnetic field, $\mathbf{B}$, that is used in all magnetohydrodynamical (MHD) problems is the induction equation. In order to derive this, we need to consider the above. By combining equations (4) and (5) we can eliminate $\mathbf{j}$,

$$\nabla \times \mathbf{B} = \mu_0 \sigma \left(\mathbf{E} + \mathbf{u} \times \mathbf{B} \right).$$

Now, taking the curl of the above which produces a $\nabla \times \mathbf{E}$ term, which equation (3) can be substituted into, giving,

$$\nabla \times \left(\frac{1}{\mu_0 \sigma} \nabla \times \mathbf{B} \right) = \nabla \times \left(\mathbf{E} + \mathbf{u} \times \mathbf{B} \right),$$

rearranging for $\partial\mathbf{B}/\partial t$, and defining $\eta = 1/\mu_0\sigma$ to be the magnetic diffusivity, gives,

$$\frac{\partial \mathbf{B}}{\partial t} = \nabla \times (\mathbf{u} \times \mathbf{B} - \eta \nabla \times \mathbf{B}), \tag{6}$$

which is the induction equation.

Now a description of the fluid motion is required. An example of such an equation for the fluid motion would be the Navier-Stokes (augmented by a Lorentz force term),

$$\frac{\partial \mathbf{u}}{\partial t} + (\mathbf{u} \cdot \nabla)\mathbf{u} + 2\boldsymbol{\Omega} \times \mathbf{u} = -\frac{1}{\rho}\nabla p + \mathbf{g} + \frac{1}{\mu_0 \rho}(\nabla \times \mathbf{B}) \times \mathbf{B} + \frac{1}{\rho}\nabla \cdot \boldsymbol{\tau}, \tag{7}$$

where $\boldsymbol{\Omega}$ is angular velocity and the term $\boldsymbol{\Omega} \times \mathbf{u}$ is the Coriolis effect, $\mathbf{g}$ is the gravitational acceleration, $\boldsymbol{\tau}$ is the viscous stress tensor, ρ is the fluid density and ∇p is the pressure gradient. Finally the additional term to the Navier-Stokes is $(\nabla \times \mathbf{B}) \times \mathbf{B}$ which is the Lorentz force term that acts back on the fluid. This equation would be then solved for $\mathbf{u}$.

However when it comes to developing a solar dynamo model, it is best to simplify the above MHD system of equations by dropping equation (7), and give an a priori form of the flow field. This means we neglect the feedback of $\mathbf{B}$ upon the flow. The resulting simplification means that the MHD induction equation is linear in $\mathbf{B}$ (see Charbonneau (2010) and Choudhuri (1998)).

2.1.1 Simplification of the MHD induction equation

There can be some simplifications made to the induction equation. Firstly if we assume η is constant, we can then use suffix notation to simplify the $\nabla \times (\nabla \times \mathbf{B})$ term in equation (6):

$$\begin{aligned} -\eta \left[\nabla \times (\nabla \times \mathbf{B})\right]_i &= -\eta \epsilon_{ijk}\epsilon_{klm}\frac{\partial B_m}{\partial x_j \partial x_l} \\ &= -\eta \epsilon_{kij}\epsilon_{klm}\frac{\partial B_m}{\partial x_j \partial x_l} \end{aligned}$$

Using the relationship between the Levi-Civita symbol and the Kronecker delta gives,

$$
\begin{aligned}
-\eta \left[\nabla \times (\nabla \times \mathbf{B})\right]_i &= -\eta \left(\delta_{il}\delta_{jm} - \delta_{im}\delta_{jl}\right) \frac{\partial B_m}{\partial x_j \partial x_l}, \\
&= -\eta \left(\delta_{il}\delta_{jm} \frac{\partial B_m}{\partial x_j \partial x_l} - \delta_{im}\delta_{jl}\right) \frac{\partial B_m}{\partial x_j \partial x_l}, \\
&= -\eta \left(\frac{\partial B_j}{\partial x_j \partial x_i} - \frac{\partial B_i}{\partial x_j \partial x_j}\right), \\
&= -\eta \left[\frac{\partial}{\partial x_i}\left(\frac{\partial B_j}{\partial x_j}\right) - \nabla^2 B_i\right].
\end{aligned}
$$

Now using Maxwell's third equation, $\nabla \cdot \mathbf{B} = 0$, gives

$$
-\eta \left[\nabla \times (\nabla \times \mathbf{B})\right]_i = \eta \nabla^2 B_i.
$$

So the MHD induction equation can be simplified (under the assumption η is constant) to,

$$
\frac{\partial \mathbf{B}}{\partial t} = \nabla \times (\mathbf{u} \times \mathbf{B}) + \eta \nabla^2 \mathbf{B}. \tag{8}
$$

This equation appears commonly in many literature on solar dynamo theory (see for example Tobias (2002) and Priest (1982)).

2.2 The Dynamo problem

For a dynamo to operate, the magnetic field must be sustained by the fluid motions whilst overcoming dissipative effects. Since the magnetic field is divergence free (Maxwell's equation), it can be split into poloidal (meridional) and toroidal (azimuthal) components, and we can regard the dynamo as a cycle in which the poloidal field is regenerated from the toroidal field and vice versa. It is important to introduce the mechanisms that allows the conversion of the poloidal field to the toroidal field and vice versa so that we understand why the dynamo problem arises.

The conversion of the poloidal to the toroidal magnetic field is called the ω-effect and is due to differential rotation in the convective zone. The large differential shearing at the tachocline causes the poloidal field lines to be wrapped around the Sun producing a toroidal field.

The conversion from toroidal to poloidal is much more difficult because there is no source term in the axisymmetric MHD equation that has the toroidal to poloidal mechanism and this the crux of Cowling's antidynamo theorem. The theorem (see Choudhuri (1998) for an outline) states an axisymmetric flow cannot sustain a steady axisymmetric magnetic field against resistive decay. This implies that any attempts to approach the solar dynamo problem would require using non-axisymmetric systems. To overcome this, there are possible non-axisymmetric mechanisms used to provide a source term to generate the poloidal field. The toroidal to poloidal conversion process is usually called the α-effect and there are several possible mechanisms that could be responsible for this process.

2.2.1 Convective α-effect

Physically the α-effect was described by Parker (1955) as localised turbulent cyclonic motions that cause the toroidal field lines to twist as they rise, due to convection, forming many small-scale poloidal flux loops. The net effect of these loops generates a global poloidal field (see figure 4).

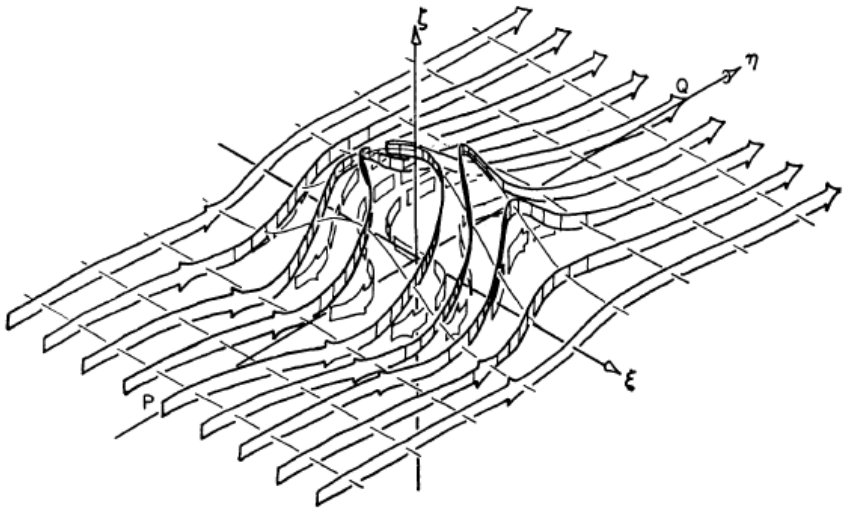

Figure 5: Parker's sketch of the α-effect (Parker, 1955)

2.2.2 MHD instabilities

Toroidal magnetic flux ropes can be stored in the tachocline, and these flux ropes are subject to the magnetic buoyancy instability. As the flux ropes rises to the photosphere through the convective zone the Coriolis effect twists the flux rope

and produces a corkscrew motion through the axis of the flux rope. This gives the twisting of the toroidal field into meridional planes. This twist is a source for the poloidal field generation with an azimuthal electromotive force (e.m.f) being produced. This is similar to Parker's idea of helical twisting of toroidal fieldlines by cyclonic convection, the subtlety being in this process we consider a buoyancy situation and not convection like in Parker's α-effect.

The weaker buoyant flux ropes do not reach the photosphere but instead are recycled into convective zone and then pumped into the tachocline via magnetic pumping (see, for example, (Priest, 1982) and (Charbonneau, 2010)).

2.2.3 The Babcock-Leighton mechanism

The Babcock-Leighton mechanism was suggested by Babcock (1961) and Leighton (1969). Meridional flow (the longitudinally averaged and radial velocity component (Stix, 2004)) and supergranulation has been observed on the surface of the Sun. It is believed that the combination of the flow and supergranulation sweeps poloidal magnetic flux towards the poles (see figure 6), with the poloidal magnetic flux being a net effect of the diffusive cancellation between sunspots of opposite polarity. The East-West tilt of sunspot pairs (Joy's law) has been observed on the surface and is thought to be the cause of dissipative effect due to the leading sunspot being closer to the equator and its polar opposite in the other hemisphere. The resulting poloidal field is advected to the tachocline as part of meridional circulation – thus we have a mechanism for the toroidal to poloidal conversion and have completed the dynamo loop.

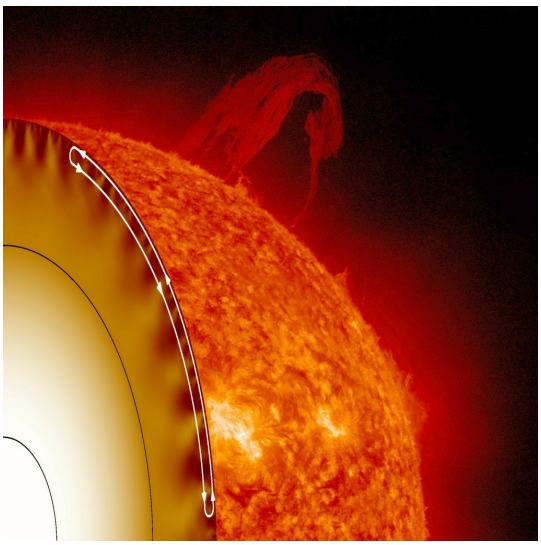

Figure 6: Meridional Circulation near the surface of the Sun[V]

[V] Figure 5 source: `http://solarscience.msfc.nasa.gov/images/MeridionalCirculation.jpg`

2.3 Mean-Field Equations

2.3.1 Mean-Field Electrodynamics

A more mathematical approach to this problem is via mean-field electrodynamics (MFE). The evolution of the large-scale magnetic field is on time scales that are longer than the turbulent time scale, so this mechanism lets the non-axisymmetric magnetic and velocity fields to be considered on the small-scale, and the net effect of the small-scale interactions produces a large-scale poloidal field under the α-effect. The large-scale fields are solved under the assumption of axisymmetry and the non-axisymmetric components are in the underlying small-scale processes which are not solved for. This avoids full 3D turbulent MHD simulations which are time consuming and require a lot of computational power. It can be shown that (see for example Charbonneau (2010)), using separation and averaging processes, the MHD induction equation for the mean component is identical to the original MHD induction equation, albeit an additional mean electromotive force term, $\boldsymbol{\mathcal{E}}$. This mean e.m.f term is induced by the fluctuating flow and field components and is the equivalent of the Reynolds stress term in the mean-field Navier-Stokes equation.

2.3.2 Reynold's decomposition

The magnetic and velocity fields can be analysed using with the Reynold's decomposition,

$$\mathbf{B} = \bar{\mathbf{B}} + \mathbf{b}',$$

$$\mathbf{u} = \bar{\mathbf{u}} + \mathbf{u}',$$

where $\mathbf{b}'$ and $\mathbf{u}'$ are the fluctuating components and $\bar{\mathbf{B}}$ and $\bar{\mathbf{u}}$ are the mean components of the magnetic and velocity field respectively. Taking the ensemble average of equation (8),

$$\left\langle \frac{\partial \mathbf{B}}{\partial t} \right\rangle = \left\langle \nabla \times (\mathbf{u} \times \mathbf{B}) + \eta \nabla^2 \mathbf{B} \right\rangle,$$

and then using the Reynold's decomposition gives,

$$\frac{\partial}{\partial t} \left\langle \bar{\mathbf{B}} + \mathbf{b}' \right\rangle = \nabla \times \left\langle (\bar{\mathbf{u}} + \mathbf{u}') \times \left(\bar{\mathbf{B}} + \mathbf{b}' \right) \right\rangle + \eta \nabla^2 \left\langle \bar{\mathbf{B}} + \mathbf{b}' \right\rangle, \tag{9}$$

and noting that $\langle \mathbf{u}' \rangle = 0 = \langle \mathbf{b}' \rangle$ and that $\langle \bar{\mathbf{B}} \rangle = \bar{\mathbf{B}}$, $\langle \bar{\mathbf{u}} \rangle = \bar{\mathbf{u}}$, produces the following,

$$\frac{\partial \bar{\mathbf{B}}}{\partial t} = \nabla \times \left\langle (\bar{\mathbf{u}} + \mathbf{u}') \times \left(\bar{\mathbf{B}} + \mathbf{b}'\right) \right\rangle + \eta \nabla^2 \bar{\mathbf{B}}. \tag{10}$$

In order to deal with the $\nabla \times \left\langle (\bar{\mathbf{u}} + \mathbf{u}') \times \left(\bar{\mathbf{B}} + \mathbf{b}'\right) \right\rangle$ term, we should consider the i^{th} component, and on expanding the terms, we have,

$$\begin{aligned}
\left[\nabla \times \left\langle (\bar{\mathbf{u}} + \mathbf{u}') \times \left(\bar{\mathbf{B}} + \mathbf{b}'\right) \right\rangle\right]_i &= \left\langle \epsilon_{ijk} \frac{\partial}{\partial x_j} \epsilon_{klm} \left(\bar{\mathrm{u}}_l \bar{\mathrm{B}}_m + \bar{\mathrm{u}}_l \mathrm{b}'_m + \mathrm{u}'_l \bar{\mathrm{B}}_m + \mathrm{u}'_l \mathrm{b}'_m \right) \right\rangle, \\
&= \left\langle \epsilon_{ijk} \frac{\partial}{\partial x_j} \epsilon_{klm} \left(\bar{\mathrm{u}}_l \bar{\mathrm{B}}_m + \mathrm{u}'_l \mathrm{b}'_m \right) \right\rangle, \\
&= \nabla \times \left(\bar{\mathbf{u}} \times \bar{\mathbf{B}} \right) + \nabla \times \left\langle (\mathbf{u}' \times \mathbf{b}') \right\rangle .
\end{aligned}$$

This now simplifies equation (10) to,

$$\frac{\partial \bar{\mathbf{B}}}{\partial t} = \nabla \times \left(\bar{\mathbf{u}} \times \bar{\mathbf{B}} \right) + \nabla \times \left\langle (\mathbf{u}' \times \mathbf{b}') \right\rangle + \eta \nabla^2 \bar{\mathbf{B}}. \tag{11}$$

We now have a term which is the electromotive force,

$$\boldsymbol{\mathcal{E}} = \langle (\mathbf{u}' \times \mathbf{b}') \rangle.$$

The e.m.f term can only be non-zero only if there is a correlation between the average fluctuating components of the velocity and magnetic field, $\mathbf{u}'$ and $\mathbf{b}'$. We can evaluate $\boldsymbol{\mathcal{E}}$ if we can express it in terms of the averaged magnetic field $\bar{\mathbf{B}}$. This can be done by finding an expression for the evolution of the fluctuating magnetic component $\mathbf{b}'$. Following a similar vein to Choudhuri (1998), this gives,

$$\boldsymbol{\mathcal{E}} = \alpha \bar{\mathbf{B}} - \beta \nabla \times \bar{\mathbf{B}}. \tag{12}$$

Where β is the turbulent diffusivity and α is the effect of fluid fluctuations. Moffat (1978) uses a more rigorous derivation and goes into further detail into what these α and β terms are for isotropic and non-isotropic fluids, and in terms of spectrum tensors. Equation (12) is for the case where we assume the fluid is isotropic. Now, for a given a priori flow, we can substitute the e.m.f term (12) into equation (11) giving,

$$\frac{\partial \bar{\mathbf{B}}}{\partial t} = \nabla \times \left(\bar{\mathbf{u}} \times \bar{\mathbf{B}}\right) + \nabla \times \left(\alpha \bar{\mathbf{B}}\right) - \nabla \times \left(\beta \nabla \times \bar{\mathbf{B}}\right) + \eta \nabla^2 \bar{\mathbf{B}}. \tag{13}$$

In order to make headway into developing a model, it is necessary that the equations describing the nature of the field (for now, the other aspects, such as toroidal to poloidal mechanisms can be approached later after the basic equations have been implemented) should be analyzed or perhaps simplified in order to begin developing a simple model.

3 A Cartesian model

The aim now is to first derive a 2D model with two scalar equations for the poloidal and toroidal components of the magnetic field $\mathbf{B}$. We will then introduce non-linear quenching terms for α, η and the velocity v. Quenching is where we parameterize a term, in this case, the α, η and velocity terms, so that we can strengthen or weaken these terms relative to the others in the equation. This nonlinearity represents (to some extent) the back-reaction of the magnetic field upon the flow. By doing this, we can see what affect individually these terms have on the evolution of the magnetic field. Once we have derived the 2D equation with appropriate non-linear quenching mechanisms we will further reduce this to a 1D model.

3.1 Poloidal and toroidal scalar equations

For the convenience of notation, the bars shall be dropped from here onwards. The magnetic field, $\mathbf{B}$, shall now be expressed in toroidal and poloidal components, under the following assumptions. Firstly we will consider 2D axisymmetric Cartesian geometry in x and z (leaving us independent of y), where x will represent latitude, z radial depth and y is the longitudinal component. In other words, we 'flatten out' the Sun and model it as a box. The boundary conditions at the north and south pole of the box will be that the magnetic field is zero.

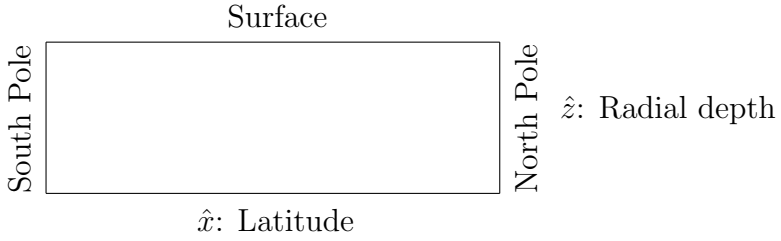

Figure 7: A schematic diagram of the Sun flattened out

We shall also take the molecular diffusivity, η, to be constant, and the turbulent diffusivity to be $\beta = \beta(x, z)$. The alpha effect will also be a function of x and z too, $\alpha = \alpha(x, z)$. Finally our velocity component will be in the longitudinal direction, $\mathbf{u} = v(x, z)\,\hat{\mathbf{y}}$. The magnetic field shall take the following form,

$$\mathbf{B} = B(x, z, t)\hat{\mathbf{y}} + \nabla \times (A(x, z, t)\hat{\mathbf{y}}),$$

where B is the toroidal component and A is the poloidal component of the magnetic field. Substituting into equation (13) gives the following,

$$\begin{aligned}
\hat{\mathbf{x}} &: \frac{\partial}{\partial t}\left(\frac{\partial A}{\partial z}\right) = \frac{\partial}{\partial z}(\alpha B) + \frac{\partial}{\partial z}\left(\beta\nabla^2 A\right) - \eta\frac{\partial}{\partial z}\left(\nabla^2 A\right) \\
\hat{\mathbf{y}} &: \frac{\partial B}{\partial t} = \frac{\partial v}{\partial z}\frac{\partial A}{\partial x} - \frac{\partial v}{\partial x}\frac{\partial A}{\partial z} - \frac{\partial}{\partial x}\left(\alpha\frac{\partial A}{\partial z}\right) - \frac{\partial}{\partial z}\left(\alpha\frac{\partial A}{\partial x}\right) \\
&\quad + \frac{\partial\beta}{\partial x}\frac{\partial B}{\partial x} + \frac{\partial\beta}{\partial z}\frac{\partial B}{\partial z} + \beta\nabla^2 B + \eta\nabla^2 B, \\
\hat{\mathbf{z}} &: \frac{\partial}{\partial t}\left(\frac{\partial A}{\partial x}\right) = \frac{\partial}{\partial x}(\alpha B) + \frac{\partial}{\partial x}\left(\beta\nabla^2 A\right) + \eta\nabla^2\left(\frac{\partial A}{\partial x}\right).
\end{aligned}$$

Now the derivative for the $\hat{\mathbf{x}}$ and $\hat{\mathbf{z}}$ components can commute such that they can both be integrated with x and z respectively,

$$\begin{aligned}
\hat{\mathbf{x}} &: \frac{\partial}{\partial z}\left(\frac{\partial A}{\partial t}\right) = \frac{\partial}{\partial z}(\alpha B) + \frac{\partial}{\partial z}\left(\beta\nabla^2 A\right) + \eta\frac{\partial}{\partial z}\left(\nabla^2 A\right), \\
\hat{\mathbf{z}} &: \frac{\partial}{\partial x}\left(\frac{\partial A}{\partial t}\right) = \frac{\partial}{\partial x}(\alpha B) + \frac{\partial}{\partial x}\left(\beta\nabla^2 A\right) + \eta\frac{\partial}{\partial x}\left(\nabla^2 A\right).
\end{aligned}$$

When integrated, each produce an arbitrary function, $f(z,t)$ and $g(x,t)$, on the other hand if they are both to be satisfied, it must be an arbitrary of time only. This gives,

$$\frac{\partial A}{\partial t} = \alpha B + \beta \nabla^2 A + \eta \nabla^2 A + h\left(t\right),$$

where $h(t)$ is an arbitrary function of integration. However, because we have no time-dependence at the poles for the magnetic field (we have the boundary condition $A = B = 0$), then it must be $h\left(t\right) = 0$. This now results in two evolution equations for the poloidal and toroidal field,

$$\frac{\partial A}{\partial t} = \alpha B + \beta \nabla^2 A + \eta \nabla^2 A, \tag{14}$$

$$\frac{\partial B}{\partial t} = \frac{\partial v}{\partial z}\frac{\partial A}{\partial x} - \frac{\partial v}{\partial x}\frac{\partial A}{\partial z} - \frac{\partial}{\partial x}\left(\alpha \frac{\partial A}{\partial z}\right) - \frac{\partial}{\partial z}\left(\alpha \frac{\partial A}{\partial x}\right) + \frac{\partial \beta}{\partial x}\frac{\partial B}{\partial x} + \frac{\partial \beta}{\partial z}\frac{\partial B}{\partial z} + \beta \nabla^2 B + \eta \nabla^2 B. \tag{15}$$

3.2 The $\alpha\omega$ approximation

Equations (14) and (15), which are the evolution equations for the poloidal and toroidal field, describe an $\alpha^2\omega$ dynamo – an α and ω process in equation (15) and an α process in equation (14). However, the α term in equation (15) shall now be neglected because of the strong differential rotation being much larger relative to the α-effect contribution in the toroidal field equation; this is the $\alpha\omega$ approximation.

With this in mind, the focus shall now return to introducing non-linear quenching terms for α, η and v and seeing how these non-linearities have an affect on the magnetic field. Firstly it should be noted that the molecular diffusivity, η (which is constant), is relatively small in comparison to the turbulent diffusivity β, so we set $\eta_T = \beta + \eta$ to be the turbulent diffusivity.

3.2.1 Introducing α, η_T and ω quenching parameters

We now introduce the following non-linear quenching terms,

$$\begin{aligned}\alpha &= \frac{\alpha\left(x,z\right)}{1+\lambda B^2},\\ \eta_T &= \frac{\eta_T\left(x,z\right)}{1+\mu B^2},\\ \nabla v &= \frac{1}{1+\nu B^2}\nabla v,\end{aligned}$$

where λ, μ and ν are the quenching parameters for the α, η_T and ω-effect respectively. It is worth noting that $1/\left(1+\nu B^2\right)$ is more of a ω quenching based on the shearing effect $\partial v/\partial z$, rather than a velocity quenching on v.

Considering the terms from equation (13). The $\nabla\times(\mathbf{u}\times\mathbf{B})$ term becomes,

$$\nabla\times(\mathbf{u}\times\mathbf{B}) = \frac{1}{1+\nu B^2}\left(\frac{\partial v}{\partial z}\frac{\partial A}{\partial x} - \frac{\partial v}{\partial x}\frac{\partial A}{\partial z}\right)\hat{\mathbf{y}}.$$

Now, for the α term,

$$\nabla\times(\alpha\mathbf{B}) = \begin{vmatrix} \hat{\mathbf{x}} & \hat{\mathbf{y}} & \hat{\mathbf{z}} \\ \partial/\partial x & 0 & \partial/\partial z \\ \frac{\alpha}{1+\lambda B^2}\left(-\frac{\partial A}{\partial z}\right) & \frac{\alpha B}{1+\lambda B^2} & \frac{\alpha}{1+\lambda B^2}\left(-\frac{\partial A}{\partial x}\right) \end{vmatrix},$$

we neglect the $\hat{\mathbf{y}}$-component as this is now an $\alpha\omega$-dynamo, giving,

$$\begin{aligned}\hat{\mathbf{x}} &: -\frac{\partial}{\partial z}\left(\frac{\alpha B}{1+\lambda B^2}\right),\\ \hat{\mathbf{z}} &: \frac{\partial}{\partial x}\left(\frac{\alpha B}{1+\lambda B^2}\right).\end{aligned}$$

The components of the final term, $\nabla\times\left(\eta_T/\left(1+\mu B^2\right)(\nabla\times B)\right)$ are,

$$
\begin{aligned}
\hat{\mathbf{x}} &: \frac{\partial}{\partial z}\left(\frac{\eta_T}{1+\mu B^2}\left(\frac{\partial^2 A}{\partial x^2}+\frac{\partial^2 A}{\partial z^2}\right)\right), \\
\hat{\mathbf{y}} &: \frac{\partial}{\partial z}\left(\frac{\eta_T}{1+\mu B^2}\left(-\frac{\partial B}{\partial z}\right)\right)-\frac{\partial}{\partial x}\left(\frac{\eta_T}{1+\mu B^2}\left(\frac{\partial B}{\partial x}\right)\right), \\
\hat{\mathbf{z}} &: \frac{\partial}{\partial x}\left(\frac{\eta_T}{1+\mu B^2}\left(-\frac{\partial^2 A}{\partial x^2}-\frac{\partial^2 A}{\partial z^2}\right)\right).
\end{aligned}
$$

Where the diffusivity term for the $\hat{\mathbf{y}}$ component can be expressed as,

$$
\frac{\eta_T}{1+\mu B^2}\left(\frac{\partial^2 B}{\partial x^2}+\frac{\partial^2 B}{\partial z^2}\right)-\eta_T\frac{2\mu B}{(1+\mu B^2)^2}\left(\left(\frac{\partial B}{\partial x}\right)^2+\left(\frac{\partial B}{\partial z}\right)^2\right).
$$

Now considering each component and using the same ideas as previously (commutativity of derivatives), we have the two evolution equations for A and B for a non-linear $\alpha\omega$ dynamo:

$$
\frac{\partial A}{\partial t}=\frac{\alpha B}{1+\lambda B^2}+\frac{\eta_T}{1+\mu B^2}\left(\frac{\partial^2 A}{\partial x^2}+\frac{\partial^2 A}{\partial z^2}\right) \tag{16}
$$

$$
\begin{aligned}
\frac{\partial B}{\partial t}=&\frac{1}{1+\nu B^2}\frac{\partial v}{\partial z}\frac{\partial A}{\partial x}-\frac{\partial v}{\partial x}\frac{\partial A}{\partial z}+\frac{\eta_T}{1+\mu B^2}\left(\frac{\partial^2 B}{\partial x^2}+\frac{\partial^2 B}{\partial z^2}\right) \\
&-\eta_T\frac{2\mu B}{(1+\mu B^2)^2}\left(\left(\frac{\partial B}{\partial x}\right)^2+\left(\frac{\partial B}{\partial z}\right)^2\right).
\end{aligned} \tag{17}
$$

Now that we have introduced these new terms, we can now alter the strength of our α, η and ω non-linearities and explore how this interacts with the magnetic field. However, we first must make these equations dimensionless.

3.3 Dimensionless equations

In order to model the $\alpha\omega$ equations, they need to be dimensionless. Following Tobias (1996), we shall consider non-dimensional scalings.

The other scalings[VI]are as follows;

$$\mathbf{x} = l\hat{\mathbf{x}}, \quad \eta_T = \eta_{T_0}, \quad \alpha = \alpha_0\hat{\alpha}\left(x, z\right),$$
$$A = \frac{l^2 B_0 \alpha_0}{\eta_{T_0}}\hat{A}, \quad B = B_0\hat{B}, \quad t = \frac{l^2}{\eta_{T_0}}\hat{t}, \quad \mathbf{v} \sim \omega_0 l\hat{\mathbf{v}}\left(x, z\right),$$

where the hat denotes the dimensionless variable. Here we are considering a box of length l, with α_0 and ω_0 being the coefficients for the dimensionless α and ω effect and η_{T_0} is the coefficient for the dimensionless turbulent diffusivity. Finally B_0 is the coefficient for the dimensionless toroidal field. There is still the case to consider how the quenching parameters μ, λ ν are expressed in dimensionless form. Here we can see that if,

$$\alpha \to \frac{1}{1 + \lambda B^2}\alpha,$$

is the dimensionless form, then λ has dimensions $1/B_0^2$, the same applies for μ and ν, and so,

$$\lambda = \frac{\hat{\lambda}}{B_0^2}, \quad \mu = \frac{\hat{\mu}}{B_0^2}, \quad \nu = \frac{\hat{\nu}}{B_0^2}.$$

Now substituting into the non-linear $\alpha\omega$ approximation (equations (16) and (17)) gives,

$$\frac{l^2\beta_0\alpha_0}{\eta_{T_0}}.\frac{\eta_{T_0}}{l}\frac{\partial\hat{A}}{\partial\hat{t}} = \frac{\alpha_0\hat{\alpha}\left(x, z\right)}{1 + \hat{\lambda}\hat{B}^2}B_0\hat{B} + \frac{\eta_{T_0}}{1 + \hat{\mu}\hat{B}^2}\left(\frac{B_0\alpha_0}{\eta_{T_0}}\left(\frac{\partial^2\hat{A}}{\partial\hat{x}^2} + \frac{\partial^2\hat{A}}{\partial\hat{z}^2}\right)\right),$$
$$\frac{B_0\eta_{T_0}}{l^2}\frac{\partial\hat{B}}{\partial\hat{t}} = \frac{\omega_0 l B_0\alpha_0}{\eta_{T_0}}\left(\frac{1}{1 + \hat{\nu}\hat{B}^2}\frac{\partial\hat{v}}{\partial\hat{z}}\frac{\partial\hat{A}}{\partial\hat{x}} - \frac{\partial\hat{v}}{\partial\hat{x}}\frac{\partial\hat{A}}{\partial\hat{z}}\right) + \frac{B_0\eta_{T_0}}{l^2\left(1 + \hat{\mu}\hat{B}^2\right)}\left(\frac{\partial^2\hat{B}}{\partial\hat{x}^2} + \frac{\partial^2\hat{B}}{\partial\hat{z}^2}\right)$$
$$- \eta_{T_0}\frac{B_0^2}{l^2}.\frac{1}{B_0}\frac{2\hat{\mu}\hat{B}}{\left(1 + \hat{\mu}\hat{B}\right)^2}\left(\left(\frac{\partial\hat{B}}{\partial\hat{x}}\right)^2 + \left(\frac{\partial\hat{B}}{\partial\hat{z}}\right)^2\right),$$

and, on simplification and removing hats for ease of notation, produces the following governing equations:

[VI]We can also note that comparing terms in the mean field equation (13), $\alpha\mathbf{B}$ has the same dimensions as $\mathbf{u} \times \mathbf{B}$, and so we have a dimensional estimate for α which is, $\alpha \sim \frac{L}{T}$, for L length and T time

$$\frac{\partial A}{\partial t} = \frac{\alpha\left(x,z\right)B}{1+\lambda B^2} + \frac{1}{\left(1+\mu B^2\right)}\left(\frac{\partial^2 A}{\partial x^2} + \frac{\partial^2 A}{\partial z^2}\right),$$
$$\frac{\partial B}{\partial t} = \mathcal{D}\frac{1}{1+\nu B^2}\left(\frac{\partial v}{\partial z}\frac{\partial A}{\partial x} - \frac{\partial v}{\partial x}\frac{\partial A}{\partial z}\right) + \frac{1}{\left(1+\mu B^2\right)}\left(\frac{\partial^2 B}{\partial x^2} + \frac{\partial^2 B}{\partial z^2}\right) - \frac{2\mu B}{\left(1+\mu B^2\right)^2}\left(\left(\frac{\partial B}{\partial x}\right)^2 + \left(\frac{\partial B}{\partial z}\right)^2\right).$$

These equations contain one dimensionless parameter $\mathcal{D}$, which is the Dynamo number, $\mathcal{D} = \alpha_0\omega_0 l^3/\eta_{T_0}^2$. The Dynamo number relates the α and ω-effect contributions to the turbulent diffusivity η_{T_0}.

3.4 Reduction to 1D

We are now in a position to model this problem, and we shall consider the 1D case. Here we will consider independence of z and x-dependence between $0 \leq x \leq 1$ with the south pole at $x = 0$, the north pole at $x = 1$ and the equator at $x = 1/2$. Due to the opposite polarity in each hemisphere, the α-effect will be represented as $\alpha\left(x\right) = \cos\left(x\pi\right)$.

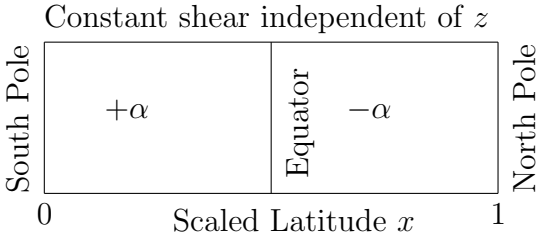

Figure 8: A simple schematic of the 1D Cartesian model used

We also set the velocity field as $v\left(z\right) \to z$. This is so that we are considering a constant shearing effect (since $\partial v/\partial z$ is independent of z and $\partial v/\partial x = 0$). Finally the poloidal and toroidal fields are set as $A \equiv A\left(x,t\right)$ and $B \equiv B\left(x,t\right)$ this gives us the following set of 1D equations.

$$\frac{\partial A}{\partial t} = \frac{\alpha B}{1+\lambda B^2} + \frac{1}{1+\mu B^2}\frac{\partial^2 A}{\partial x^2}, \tag{18}$$
$$\frac{\partial B}{\partial t} = \frac{\mathcal{D}}{1+\nu B^2}\frac{\partial A}{\partial x} + \frac{1}{1+\mu B^2}\frac{\partial^2 B}{\partial x^2} - \frac{2\mu B}{\left(1+\mu B^2\right)^2}\left(\frac{\partial B}{\partial x}\right)^2. \tag{19}$$

4 Linear analysis

The coupled toroidal and poloidal equations can be linearized. This linearized system has exponentially growing or decaying solutions. We can use linear theory to find the critical value of $\mathcal{D}$ for onset of dynamo action, $\mathcal{D}_{crit}$, and determine what symmetry (about $x = 1/2$) we expect at this onset.

The two most important symmetries we will be considering are the dipole and quadrupole symmetry. The magnetic dipole symmetry is symmetric about $x = 1/2$ in the poloidal field (A) and antisymmetric in the toroidal field (B), whilst the quadrupole symmetry is antisymmetric in the poloidal field (A) and symmetric in the toroidal field (B) (Jennings and Weiss, 1991).

First let us consider each equation individually. For equation (18), we can express this as,

$$\frac{\partial A}{\partial t} = \alpha B \left(1 + \lambda B^2\right)^{-1} + \left(1 + \mu B^2\right)^{-1} \frac{\partial^2 A}{\partial x^2}.$$

Now for small B this becomes,

$$\frac{\partial A}{\partial t} = \alpha B \left(1 - \lambda B^2\right) + \left(1 - \mu B^2\right) \frac{\partial^2 A}{\partial x^2},$$

and terms of $\mathcal{O}\left(B^2\right)$ are ignored giving the linearised equation,

$$\frac{\partial A}{\partial t} = \alpha B + \frac{\partial^2 A}{\partial x^2}. \tag{20}$$

Using the same idea, the linearised equation for (19) is,

$$\frac{\partial B}{\partial t} = \mathcal{D}\frac{\partial A}{\partial x} + \frac{\partial^2 B}{\partial x^2}. \tag{21}$$

For this system, our boundary conditions for this system motivates the choice for A and B in the range $0 \leq x \leq 1$ to be a set of sine expansions.

$$A = \sum_{i=1}^{n} a_n(t) \sin(n\pi x),$$
$$B = \sum_{i=1}^{n} b_n(t) \sin(n\pi x).$$

This is because we need to satisfy at the poles $x = 0$ and $x = 1$,

$$A = B = 0.$$

We initially considered the $n = 2$ case which can be calculated by hand, and this gave $\mathcal{D}_{crit} = -292.23$. Nevertheless, we expect this to be a poor approximation due to the lack of terms that have been used in this expansion. This was also the true for $n = 4$ (calculated using Matlab). So we now consider the case for a $n = 6$ expansion, and substituting these into (20) and (21), and noting $\alpha(x) = \cos(\pi x)$, gives us two coupled equations.

$$\sum_{i=1}^{n} a_n' \sin(n\pi x) = \cos(\pi x) \sum_{i=1}^{n} b_n \sin(n\pi x) - \pi^2 \sum_{i=1}^{n} n^2 a_n \sin(n\pi x),$$
$$\sum_{i=1}^{n} b_n' \sin(n\pi x) = \mathcal{D}\pi \sum_{i=1}^{n} n a_n \cos(n\pi x) - \pi^2 \sum_{i=1}^{n} n^2 b_n \sin(n\pi x).$$

I.e.

$$\sum_{i=1}^{n} a_n' \sin(n\pi x) = \sum_{i=1}^{n} \left[b_n \cos(\pi x) \sin(n\pi x) - \pi^2 n^2 a_n \sin(n\pi x) \right],$$
$$\sum_{i=1}^{n} b_n' \sin(n\pi x) = \sum_{i=1}^{n} \left[\mathcal{D}\pi n a_n \cos(n\pi x) - \pi^2 n^2 b_n \sin(n\pi x) \right].$$

These coupled equation can then projected onto Fourier modes. By multiplying each equation in turn by $\sin(n\pi x)$ and integrating over the domain, we get two sets of coupled ode's. The first set relates to the dipole symmetry,

$$
\begin{aligned}
&a_1' + \pi^2 a_1 - \frac{1}{2} b_2 = 0 \\
&b_2' + 4\pi^2 b_2 - \frac{8\mathcal{D}}{3} a_1 + \frac{24\mathcal{D}}{5} a_3 + \frac{40\mathcal{D}}{21} a_5 = 0, \\
&a_3' + 9\pi^2 a_3 - \frac{1}{2} b_2 - \frac{1}{2} b_4 = 0, \\
&b_4' + 16\pi^2 b_4 - \frac{16\mathcal{D}}{15} a_1 - \frac{48\mathcal{D}}{7} a_3 + \frac{80\mathcal{D}}{9} a_5 = 0, \\
&a_5' + 25\pi^2 a_5 - \frac{1}{2} b_4 - \frac{1}{2} b_6 = 0, \\
&b_6' + 36\pi^2 b_6 - \frac{24\mathcal{D}}{35} a_1 - \frac{8\mathcal{D}}{3} a_3 - \frac{120\mathcal{D}}{11} a_5 = 0,
\end{aligned}
$$

and the second set relates to the quadrupole symmetry,

$$
\begin{aligned}
&b_1' + \pi^2 b_1 + \frac{8\mathcal{D}}{3} a_2 + \frac{16\mathcal{D}}{15} a_4 + \frac{24\mathcal{D}}{35} a_6 = 0, \\
&a_2' + 4\pi^2 a_2 - \frac{1}{2} b_1 - \frac{1}{2} b_3 = 0, \\
&b_3' + 9\pi^2 b_3 - \frac{24\mathcal{D}}{5} a_2 + \frac{48\mathcal{D}}{7} a_4 + \frac{8\mathcal{D}}{3} a_6 = 0, \\
&a_4' + 16\pi^2 a_4 - \frac{1}{2} b_3 - \frac{1}{2} b_5 = 0, \\
&b_5' + 25\pi^2 b_5 - \frac{40\mathcal{D}}{21} a_2 - \frac{80\mathcal{D}}{8} a_4 + \frac{120\mathcal{D}}{11} a_6 = 0, \\
&a_6' + 36\pi^2 a_6 - \frac{1}{2} b_5 = 0.
\end{aligned}
$$

If we consider the quadrupolar set of equations, the time dependent coefficients take the form,

$$
\begin{aligned}
&\hat{a} \exp st, \\
&\hat{b} \exp st,
\end{aligned}
$$

where $s = \sigma + i\omega$, $\sigma, \omega \in \mathbb{R}$ and $\hat{a}$ and $\hat{b}$ are amplitudes for a and b. The derivatives transform as,

$$
\frac{\mathrm{d}}{\mathrm{d}t} \to s.
$$

Now the above can be solved in the linear matrix equation,

$$\mathrm{M}\mathbf{x} = \mathrm{B},$$

where,

$$\mathbf{x} = \begin{bmatrix} \hat{b}_1 \\ \hat{a}_2 \\ \hat{b}_3 \\ \hat{a}_4 \\ \hat{b}_5 \\ \hat{a}_6 \end{bmatrix}, \mathrm{B} = \mathbf{0},$$

and M is a 6x6 matrix containing the coefficients. By taking the determinant of M we can find the characteristic equation for s which can be solved in Matlab.

Solving the characteristic equation for $s = 0$ gives the value for onset of dynamo action, this value is also referred to as the critical Dynamo number, $\mathcal{D}_{crit} = -393.17$. At this value we should expect to see onset for a quadrupole steady state. We encountered that this is the first mode for onset of dynamo action, as the oscillatory dipole mode is found to be at $\mathcal{D} = -2671.34$.

5 Numerical results

We have used linear analysis to find the values of which we expect to see onset of dynamo action in the negative $\mathcal{D}$ regime, now we are ready to model equations (18) and (19) using FORTRAN.

5.1 Numerical methods

We can numerically solve partial differential equations using a forward time centered space finite-difference approximation (FTCS scheme) (Press, 1992), first we define a mesh containing the t- and x-axes,

$$\begin{aligned} x_j &= x_0 + j\Delta x, \quad j = 0, 1, \ldots, J \\ t_n &= t_0 + n\Delta t, \quad n = 0, 1, \ldots, N. \end{aligned}$$

where x_0 represents the boundary condition, and t_0 is the initial condition. Schematically our mesh grid is as follows:

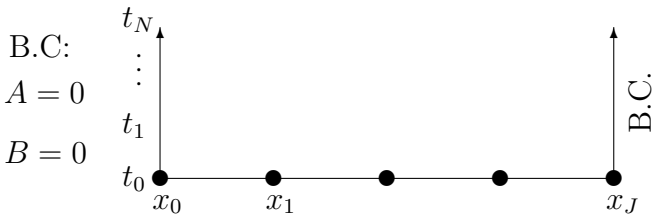

Initial condition: Pseudo-random

The initial conditions are pseudo-random, using a sum of sine functions with small amplitudes. The Euler approximation for time derivatives is,

$$\left.\frac{\partial A}{\partial t}\right|_{j,n} = \frac{A_j^{n+1} - A_j^n}{\Delta t} + \mathcal{O}\left(\Delta t\right),$$

and for spatial derivatives,

$$\left.\frac{\partial A}{\partial x}\right|_{j,n} = \frac{A_{j+1}^n - A_{j-1}^n}{2\Delta x} + \mathcal{O}\left(\Delta x^2\right),$$

where $A_j^n = A\left(t_n, x_j\right)$. We will also use a 4^{th} order Runge-Kutta time-stepping regime which is is accurate to order $\mathcal{O}\left(\Delta t^5\right)$,

$$\begin{aligned} x_{n+1} &= x_n + \frac{1}{6}\Delta t\left(k_1 + k_2 + k_3 + k_4\right), \\ t_{n+1} &= t_n + \Delta t, \end{aligned}$$

where,

$$\begin{aligned} k_1 &= A\left(t_n, x_n\right), \\ k_2 &= A\left(t_n + 1/2\Delta t, x_n + \Delta t/2k_1\right), \\ k_3 &= A\left(t_n + 1/2\Delta t, x_n + \Delta t/2k_2\right), \\ k_4 &= A\left(t_n + \Delta t, x_n + \Delta t k_3\right). \end{aligned}$$

5.1.1 von Neumann stability

It must be noted that the scheme we have used for numerically solving the PDE's could be unstable and we must make sure our timestepping size, Δt, and mesh grid size, Δx, satisfy the stability condition,

$$\frac{\Delta t}{(\Delta x)^2} \lesssim 1. \tag{22}$$

Physically, this condition is the greatest allowed timestep, which is the diffusion time across the mesh of width Δx (Press, 1992), so we shall have to consider smaller timestep sizes when we increase the diffusion rate in our system - i.e. increasing the η-quenching parameter μ. In our numerical analysis, we have taken 300 grid points across our x-domain to make sure we have a high enough resolution when dealing with high values of $\mathcal{D}$. We now have (18) and (19) appropriately coded into FORTRAN and can begin examining the effects of our non-linear quenching mechanisms.

5.2 α-quenching

We now examine the case for α-quenching and explore further values of the dynamo number and see what magnetic pole structures we get by examining output produced for the toroidal field.

5.2.1 Polewards migrating waves

If we consider the parameter space for $\mathcal{D} > 0$, we notice that increasing $\mathcal{D}$ results in toroidal magnetic activity that migrates away from the equator (see figure 9) - this is not a feature of the Sun's magnetic field and so our attention should be focused on $\mathcal{D} < 0$ (Tobias, 1997). In figure 9 we can see that we have oscillatory dynamo action – this is an oscillatory quadrupole mode as it is symmetric about the equator for the toroidal field. However it is not does not have the physical features we want; the toroidal magnetic activity is migrating towards the poles rather than towards to the equator.

In figure 9 the purple areas on the heat map represent negative polarity, with the darkest patches being the strongest negative polarity. The yellow areas represent positive polarity with the brightest being the strongest positive polarity.

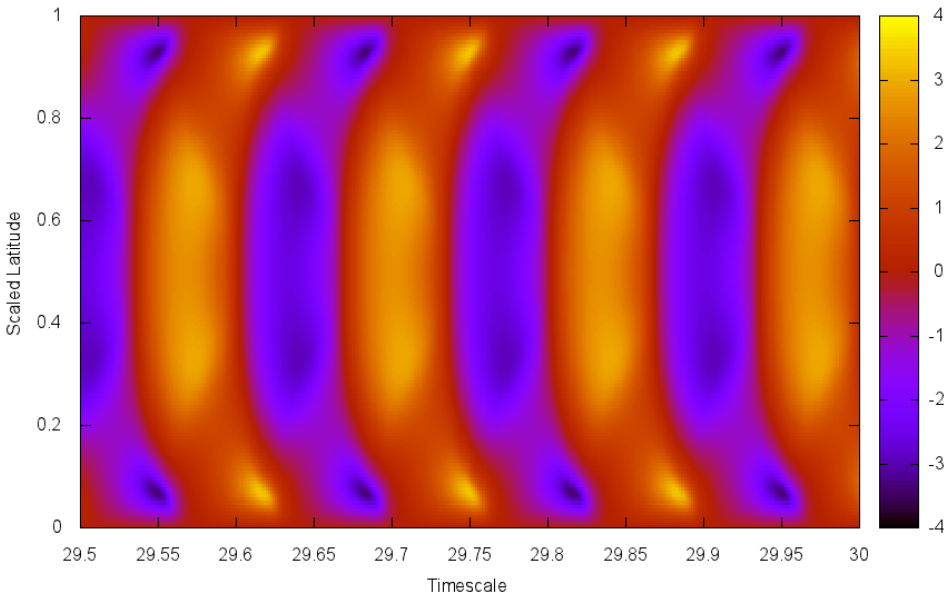

Figure 9: Toroidal field for $\mathcal{D} = 5000$, $\nu = 0, \mu = \lambda = 1$

5.2.2 Equatorial migrating waves

From our results we have found that the critical dynamo number, the value in which the onset of dynamo action begins to occur, $\mathcal{D}_{crit}$, is found to be approximately -400 for the negative regime, this value is also validated by our linear analysis.

We have explored values in the $\mathcal{D} < 0$ regime for α-quenching and there were no simple oscillatory modes; most of the solutions found were in a mixed parity state. We decided to concentrate our efforts on the combination of ω- and η-quenching and taking $\lambda = 0$ to 'turn off' the α-quenching non-linearity mechanism.

5.3 ω- and η-quenching

We now examine the effect of the combination of the ω- and η-quenching parameters, ν and μ. First we shall consider fixed quenching (of ω and η) and explore the effects of increasing and decreasing $\mathcal{D}$, then we shall consider the effects of increasing the strength of η-quenching whilst fixing the ω-quenching parameter to $\nu = 1$. As we increase the magnitude of $\mathcal{D}$ ($\mathcal{D} < 0$ regime), we are increasing the relative

strength of the α-effect and ω-effect contribution relative to the diffusivity. We expect that for lower magnitudes of $\mathcal{D}$ that the field cannot sustain itself – the diffusivity contribution overrides the inductive effects of the magnetic field and causes decay. For the linear system, we calculated $\mathcal{D}_{crit}$ to be -393.17, so values greater than this in magnitude should produce steady modes. The steady mode occurs when the inductive and dissipative effects are balanced, and the magnetic field is sustained. After further increasing of $\mathcal{D}$ we begin to observe steady modes at approximately -400 as mentioned earlier, figure 10 is an example of a steady quadrupole mode at $\mathcal{D} = -420$.

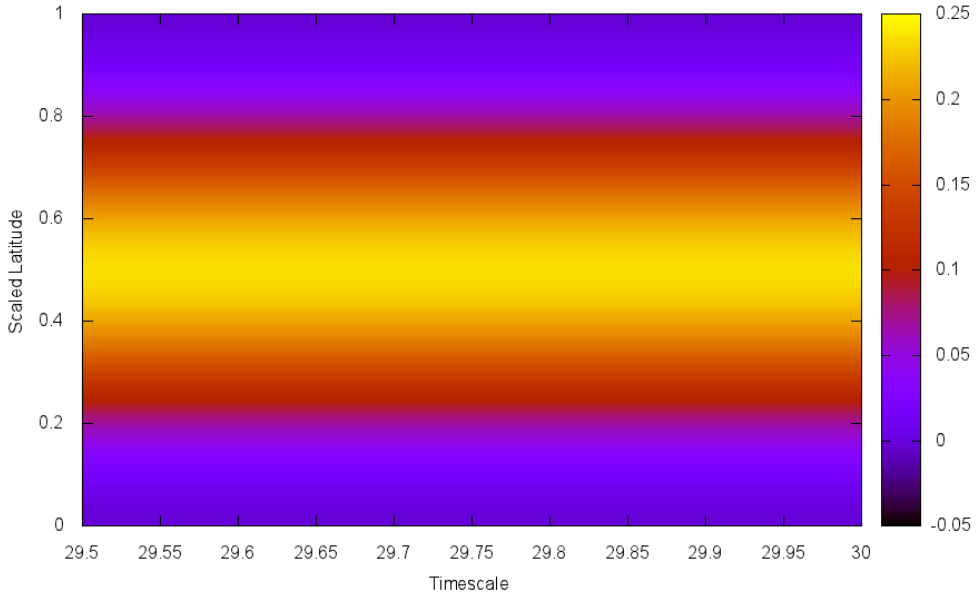

Figure 10: A steady mode at $\mathcal{D} = -420, \lambda = 0, \mu = 1, \nu = 1$. This is close to our critical value for onset $\mathcal{D}_{crit} \sim -400$

In figure 10 we see clearly a symmetric structure about the equator (the equator corresponds to scaled latitude at 0.5) with a positive polarity in the mid latitudes and a very weak positive polarity in the polar regions. This value of $\mathcal{D}$ was ran for long enough to observe its long term behaviour, this output shows that the magnetic field has not decayed after an extended period of time.

For higher values of $|\mathcal{D}|$ (> 3350), we produce oscillatory modes. The classification of the oscillatory modes determines the nature of the magnetic field which was described earlier, the first oscillatory mode we encounter has a dipole symmetry.

Figure 11 highlights this dipole symmetry – the output produced is from the toroidal

field and is antisymmetric about the equator. We can see that with each cycle, each hemisphere swaps polarity. This mimics the basic magnetic field evolution in the Sun; an 11 year solar cycle and a 22 year magnetic cycle of alternating polarity. However, it does lack many of the other features that the solar magnetic field has.

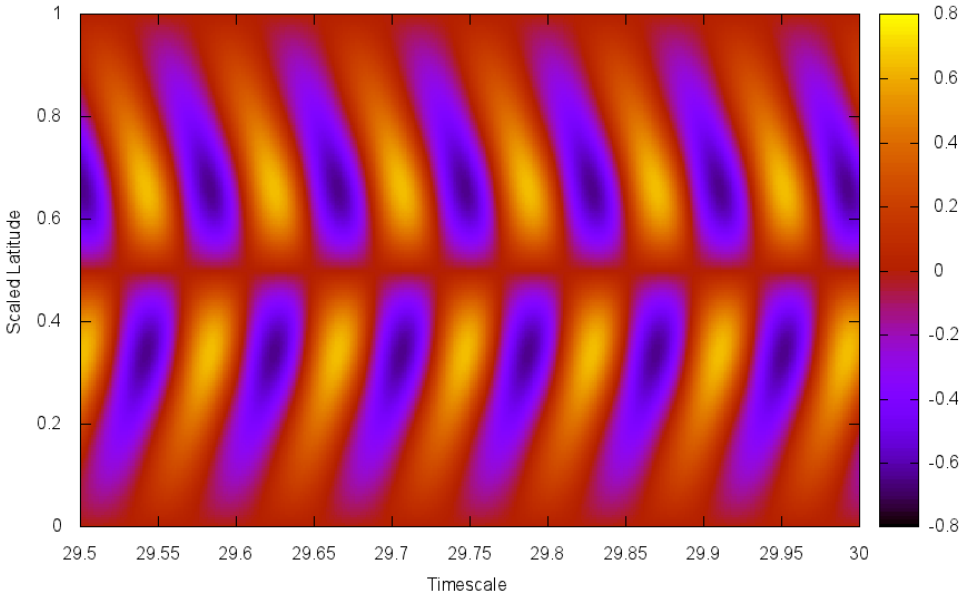

Figure 11: An oscillatory dipole mode for $\mathcal{D} = -3700, \lambda = 0, \mu = 0, \nu = 1$

For oscillatory modes in general we find that the period of oscillation decreases whilst $\mathcal{D}$ increases. The dynamo number,

$$\mathcal{D} = \frac{\alpha_0 \omega_0}{\eta_{T_0}^2},$$

as mentioned, relates the α and ω-effect contributions to the turbulent diffusivity η_{T_0}. We can see that if we increase $\mathcal{D}$, then the magnitude of the inductive contribution, $\alpha_0\omega_0$, will be greater than previously. Physically this means a combination of stronger differential shearing and the α-effect results in shorter diffusion times. Thus the correlation timescale for the magnetic field will be shorter with increasing $\mathcal{D}$. This is due to the fact that the strength of the induction outweighs the diffusion and so the rate at which the magnetic field regenerates will be much quicker. Figure 12 illustrates this decrease in period of oscillation.

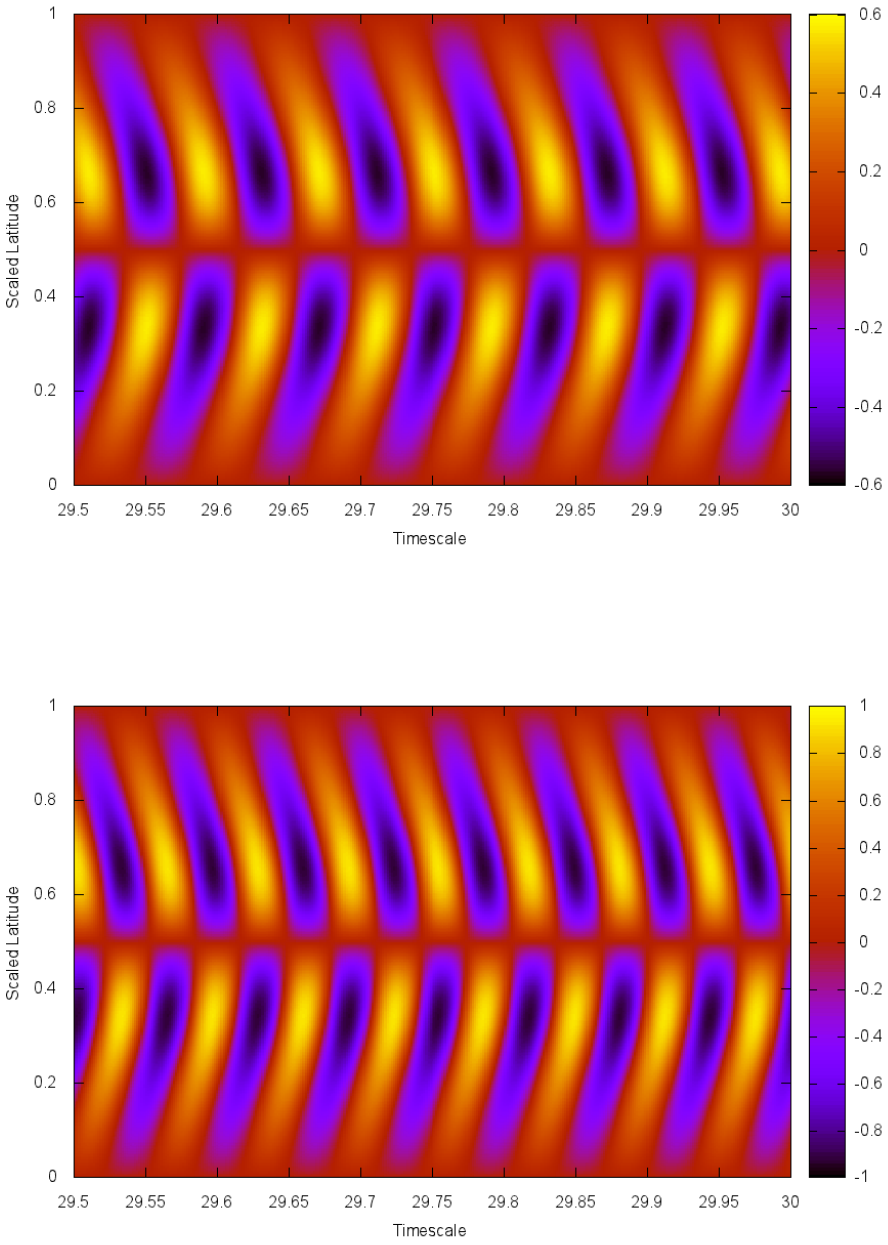

Figure 12: Comparison of oscillatory dipole modes. Top: An oscillatory mode at $\mathcal{D} = -4000, \lambda = 0, \mu = 1, \nu = 1$. Bottom: An oscillatory mode at $\mathcal{D} = -6000, \lambda = 0, \mu = 1, \nu = 1$. We can see a decrease in period of oscillation as we increase $\mathcal{D}$.

The oscillatory dipole mode ranges from approximately $-3360 \leq \mathcal{D} \leq -16000$. Very high values of $|\mathcal{D}|$ (> 16000) produces oscillatory quadrupole modes (see figure 13). There is a definite symmetric structure about the equator, with the polarity being the same throughout both hemispheres and alternating on each cycle. We can also see that there is a much stronger magnetic polarity at the equator than at mid latitudes and at the poles.

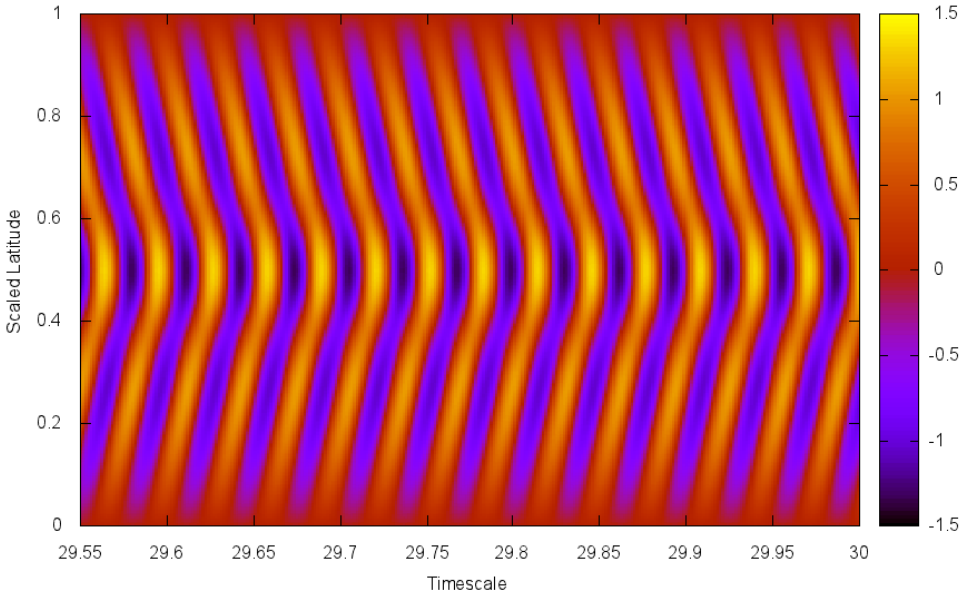

Figure 13: If we continue to increase $\mathcal{D}$ we begin to observe oscillatory quadrupolar modes. Here is an example of an oscillatory quadrupole mode at $\mathcal{D} = -16200, \lambda = 0, \mu = 1, \nu = 1$.

We stopped our investigation of $|\mathcal{D}|$ beyond values greater than 16500. At much higher values of $\mathcal{D}$ we require a greater resolution in Δx and this requires a smaller timestepping size Δt to satisfy the stability criterion (22). This leads to longer computational times, which was decided to be an unnecessary time consuming exercise given the fact we have established the values of the first few modes, and we are not particularly interested in complex magnetic structures beyond oscillatory quadrupoles.

5.3.1 Varying the strength of η-quenching

We now examine the effect of the non-linear η-quenching term that was introduced as,

$$\eta_T = \frac{\eta_T}{1 + \mu B^2}.$$

It is also worth noting again that the ω-quenching parameter will be fixed at $\nu = 1$ from now onwards. Overall we are therefore looking at the following coupled system,

$$\begin{aligned}
\frac{\partial A}{\partial t} =& \alpha B + \frac{1}{1 + \mu B^2} \frac{\partial^2 A}{\partial x^2}, \\
\frac{\partial B}{\partial t} =& \frac{\mathcal{D}}{1 + B^2} \frac{\partial A}{\partial x} + \frac{1}{1 + \mu B^2} \frac{\partial^2 B}{\partial x^2} - \frac{2\mu B}{(1 + \mu B^2)^2} \left(\frac{\partial B}{\partial x} \right)^2.
\end{aligned}$$

For fixed $\mathcal{D}$ we found that increasing μ decreased the period of oscillation, a similar behaviour to when we increased $\mathcal{D}$ (see 5.3). When we increased the strength of the quenching we began to see a shift towards the oscillatory quadrupole mode. Increasing μ appears to increase the overall effectiveness of $\mathcal{D}$, even though $\mathcal{D}$ is independent of μ. The introduction of the non-linearity has changed the effect of diffusivity in the system.

Further quenching, to $\mu = 20$, clearly shifts the dipole mode to a quadrupole mode. This shift is due to the fact we have suppressed the diffusion non-linearity. Even though μ is independent of our dynamo number, suppressing the diffusion term has indirectly reduced the relative strength of η_T compared to $\alpha_0\omega_0$. An example of a shift from dipole to quadrupole mode for $\mathcal{D} = -3800$ can be seen overleaf in figure 14. In these two outputs we can see that we have an oscillatory quadrupole solution for a value of $\mathcal{D}$ as low as -3800, with weaker η-quenching we would not see this until $|\mathcal{D}| \sim 16000$. There is also a clear reduction in period of oscillation.

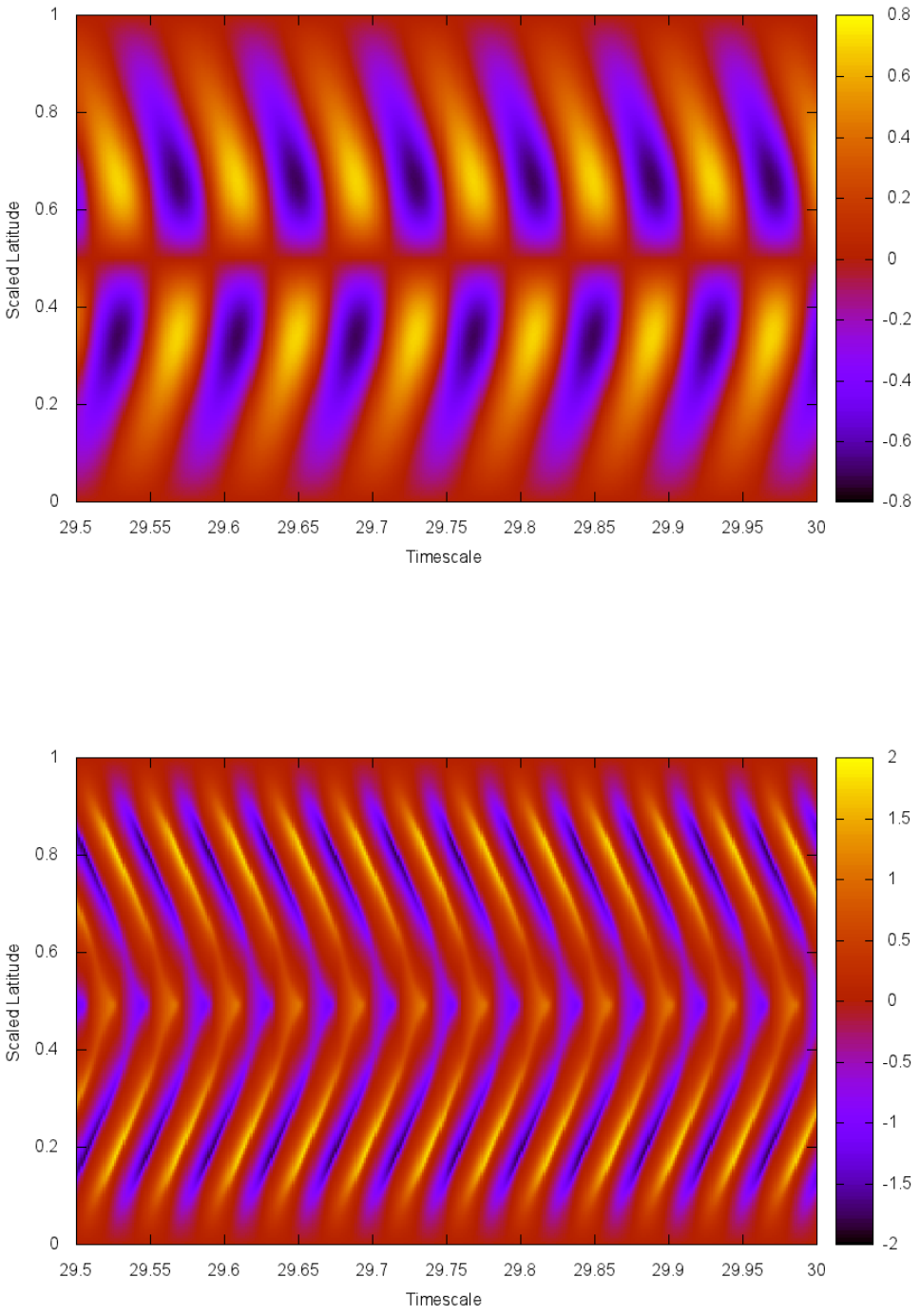

Figure 14: A comparison of $\mathcal{D} = -3800, \lambda = 0, \nu = 1$ for varying μ. Top: $\mu = 1$ gives a dipole symmetry. Bottom: $\mu = 20$ has shifted to a quadrupole mode.

We can now see that for varying μ we can produce different solution modes for the same dynamo number. It is also noticed that changing the initial conditions can also affect the modes that we observe, we now focus our attention on experimenting with initial conditions for our model and see what results occur.

5.4 Tracking solution branches

Using ideas similar to Jennings and Weiss (1991) we now follow solution branches in parameter space. This is achieved by using the final output of each run and using this as the new initial condition for the next run and then a new dynamo number is used. By slowly decreasing $\mathcal{D}$ it is possible to find overlapping solution branches, showing that different initial conditions can produce different modes and reveal regions of bistability.

Our aim now is to see what effect η-quenching has on these regions of bistability. In figure 15 below we have compared output from $\mathcal{D} = -1695$ for $\mu = 10$, the first graph shows a solution generated from pseudo-random initial conditions, whilst the second graph shows output that has been tracked back on the oscillatory branch. This shows we have found a region of bistability (an overlap) at $\mathcal{D} = -1695$; solutions in this regions are affected by the initial conditions and can favour different modes.

Further investigation of parameter space for μ reveals that the regions of bistability are very small for low values of μ. We continue tracking branches back for various values of μ, and in figures 16, 18 and 19 these branches are displayed graphically to show the overlaps in parameter space for $\mathcal{D}$.

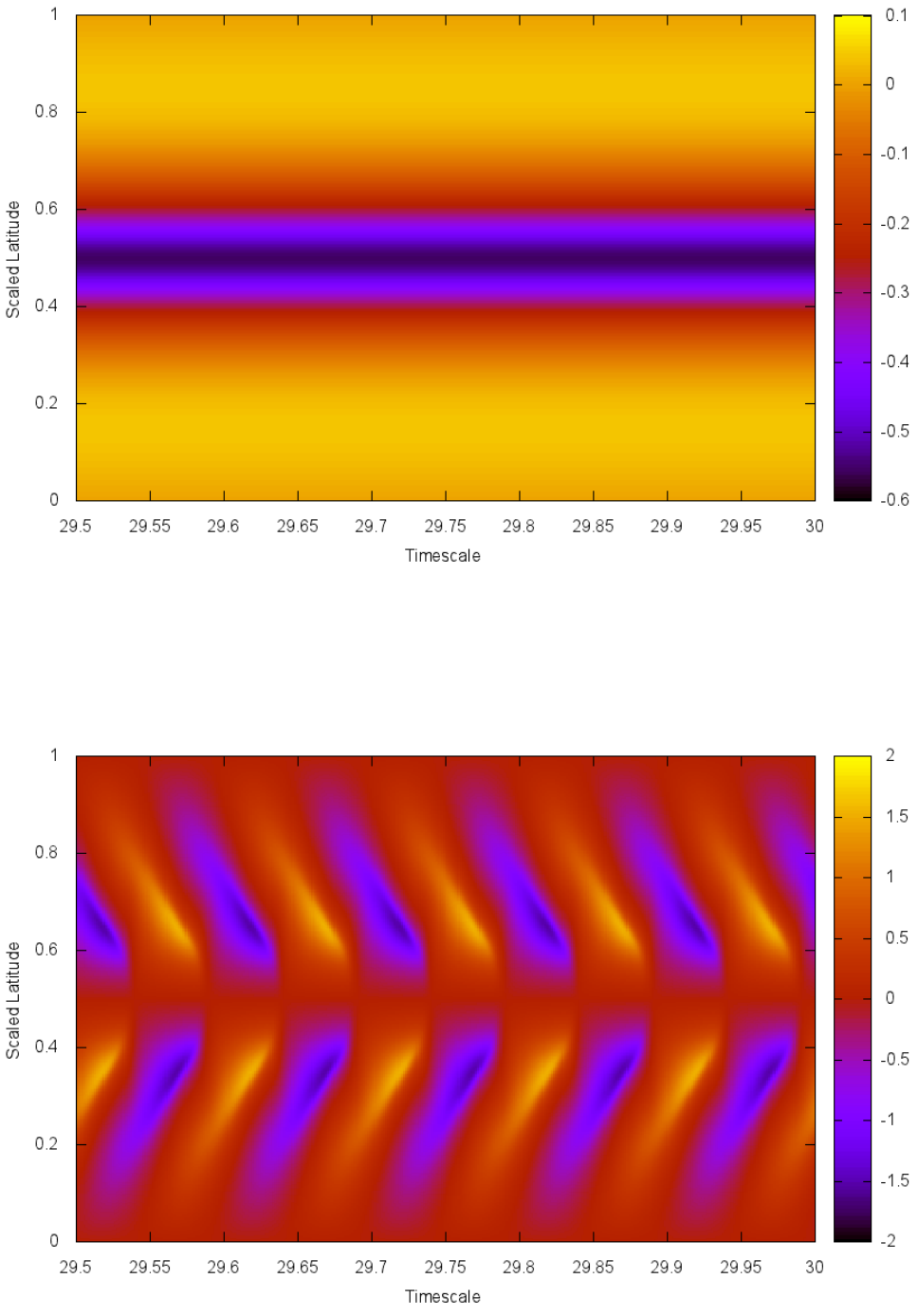

Figure 15: Toroidal field at $\mathcal{D} = -1695, \lambda = 0, \mu = 10, \nu = 1$. Top: Using pseudo-random initial conditions. Bottom: Using the final output from the previous run as the initial condition (tracked back).

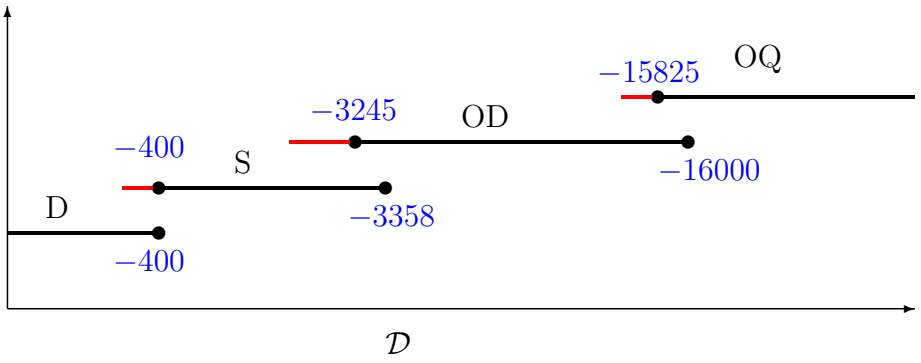

Figure 16: Bifurcation diagram for $\mu = 1$. Abbreviations: (OQ) Oscillatory quadrupole, (OD) Oscillatory dipole, (S) Steady, (D) Decay (subcritical regime).

In figure, 16, the x-axis values represents the increasing value of $|\mathcal{D}|$, the blue numbers represent the transition values when a solution branch begins or ends, and the red line represents a transition phase between two branches where it is in a mixed state between the two solutions (see figure 17).

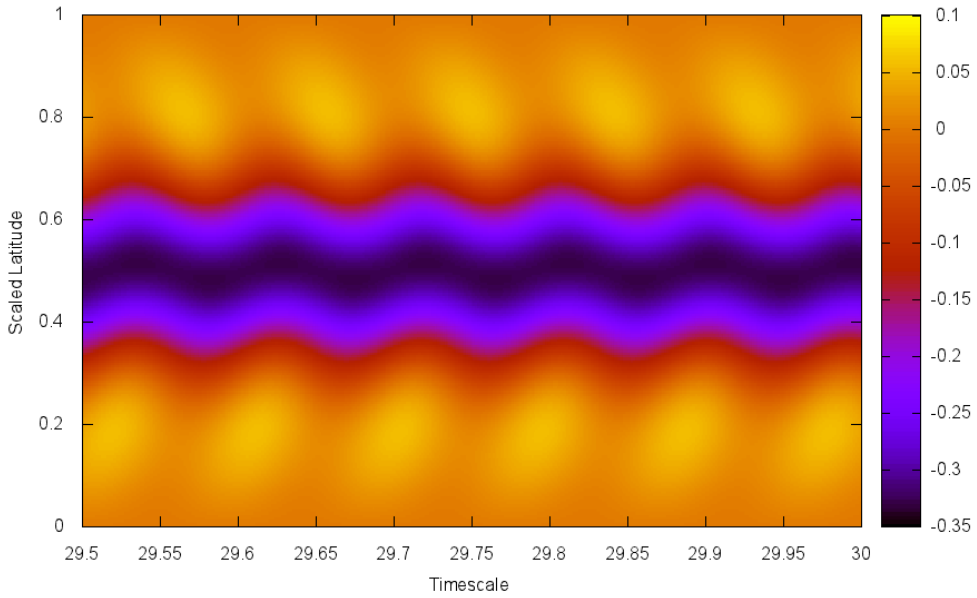

Figure 17: An example of transition at $\mathcal{D} = -3150, \lambda = 0, \mu = 1, \nu = 1$

For the $\mu = 1$ case we can see that there is some small overlap between different branches. As we track a solution back on the oscillatory quadrupole branch (OD) we find that this solution branch continues into the oscillatory dipole parameter space, what is happening is that in this range for $\mathcal{D}$ we have a region of bi-stability. In this region, depending on our initial condition we can have different mode solutions, for example we can see a bi-stability region for $-16000 \leq \mathcal{D} \leq -15825$ in which we can have an oscillatory quadrupole or an oscillatory dipole solution.

If we continue to track the oscillatory dipole branch we then overlap the steady branch with some minor transition period after. However there is no clear and definite overlap from steady to the subcritical regime, although there is a minor transition period, which may suggest there could be the possibility of an overlap for higher values of μ.

5.4.1 Dynamo action in the subcritical regime

We now investigate the effect of increasing the strength of η-quenching and in figures 18 and 19, we have included bifurcation diagrams for when we increase the strength of the η-quenching parameter to the values $\mu = 10$ and $\mu = 20$.

By increasing η-quenching by a factor of 10, we can clearly see regions of bistability (figure 18). The transitions are all but immediate when we drop to the next branch, and the overlaps between modes have increased in size. It appears η-quenching increases the size of the bistability region. However, the most important result we have from this is the overlap of the steady branch into the subcritical regime. This means we have dynamo action for $\mathcal{D} < \mathcal{D}_{crit}$ – the linear theory suggests that we cannot have dynamo action below this value, but in our non-linear model we have shown otherwise. For $\mu = 10$, we see dynamo action at -345 and for $\mu = 20$ at -289, this which the linear theory did not predict.

At $\mu = 20$, we have a very large bistability region, with the oscillatory quadrupole branch almost overlapping the whole oscillatory dipole branch. If we were to increase μ even more, it may be possible that this region could extend into the steady mode and create a region of tristability, and possibly oscillatory dynamo action in the sub-critical regime. We finally stop here, as further quenching required long computational times, although it would be interesting to see whether oscillatory dynamo action can occur in the subcritical regime.

We have seen that increasing η-quenching relates to increasing bistability regions, which leads us to the fact that initial conditions are not so important when we model the solar dynamo. It is shown that introducing η-quenching means we can have different solutions depending on the initial conditions given.

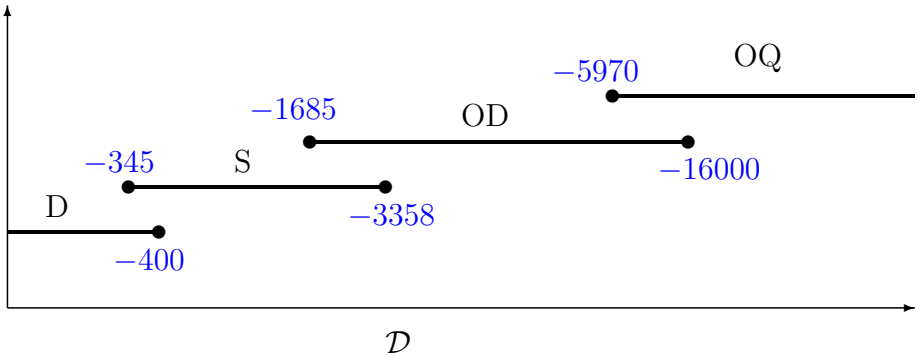

Figure 18: Bifurcation diagram for $\mu = 10$. There is dynamo action for $\mathcal{D} < \mathcal{D}_{crit}$

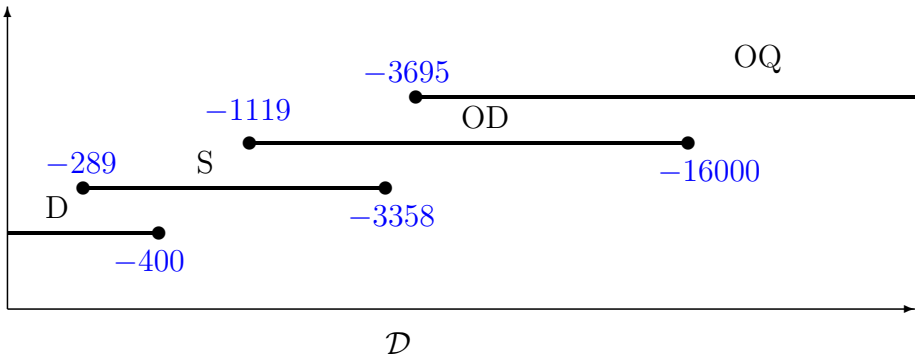

Figure 19: Bifurcation diagram for $\mu = 20$. The dynamo action continues further into the subcritical regime, and the oscillatory quadrupole branch is close to overlapping into the steady branch.

6 Conclusions

To conclude, we have taken the poloidal and toroidal field equations derived from the MHD induction equation and linearised to find what values we expect to see the onset of dynamo action. We then introduce non-linear quenching terms to see what affect the α, η and ω-effect has on the evolution of the Sun's magnetic field. By considering varying η-quenching and fixed ω-quenching, we see that an increase in strength for η-quenching increases the 'effectiveness' of $\mathcal{D}$ – we see dynamo action below $\mathcal{D}_{crit}$.

In this model, we find that the the magnetic field evolution is dependent upon initial conditions, and can produce different output. Taking this into account, we track solution branches in parameter space and find that we have regions of bi-stability and these regions increase in size the more we quench η. For example we have shown that we can produce a steady mode when a different initial condition would have produced an oscillatory mode or a decay mode, it is important to bear this in mind when we try to model the Sun's magnetic field.

Of course there are some limitations to the model used, firstly, a 1D Cartesian geometry is quite a simplistic attempt to model the solar dynamo – it provides some insight, but lacks the realism of many of the physical features that we do know about the Sun. This leads to the second point of the lack of some of physical features of the Sun. There are many features that are missing from this model which have been described in this report – a realistic differential rotation profile, a radial dependence that models the tachocline sufficiently well, and perhaps a meridional flow that could include a Babcock-Leighton mechanism.

As a final thought, it may even be possible to quench η to a point where we begin to see oscillatory solution branches overlapping into the subcritical regime – is it possible to produce oscillatory dynamo action for $\mathcal{D} < \mathcal{D}_{crit}$? If so, what value of μ must we set to achieve this?

Future work after this project could be to see what happens when we investigate a 2D model with more realistic properties such as introducing a flow to the model, or perhaps a more suitable geometry (spherical coordinates). It would be interesting to see what effect competing non-linearities have with each other, now that we have seen how η-quenching behaves, how would it behave if we begin to alter ω-quenching?

References

H.W. Babcock. The Topology of the Sun's Magnetic Field and the 22-Year Cycle. *Astrophysical Journal*, 133:572, 1961.

P. Charbonneau. Dynamo Models of the Solar Cycle. *Living Reviews in Solar Physics*, 7:3, 2010.

A.R. Choudhuri. *The Physics of Fluids and Plasmas: an introduction for astrophysicists*. 1998.

T.G. Cowling. The Magnetic Field of Sunspots. *Monthly Notices of the Royal Astronomical Society*, 94:39, 1935.

J. A. Eddy. The Maunder Minimum. *Science*, 192:1189, 1976.

G. E. Hale, F. Ellerman, S. B. Nicholson, and A. H. Joy. The Magnetic Polarity of Sun-Spots. *Astrophysical Journal*, 49:153, 1919.

R. L. Jennings and N. O. Weiss. Symmetry breaking in stellar dynamos. *Monthly Notices of the Royal Astronomical Society*, 252:249, 1991.

J.Mason, D.W. Hughes, and S.M. Tobias. The competition in the solar dynamo between surface and deep-seated alpha-effects. *The Astrophysical Journal*, 580: 89, 2002.

McGraw-Hill. McGraw-Hill Dictionary of Scientific and Technical terms, 2003.

H.K Moffat. Magnetic Field Generation in Electrically Conducting Fluids, 1978.

E. N. Parker. The formation of sunspots from the solar toroidal field. *Astrophysical Journal*, 121:491, 1955.

E. N. Parker. Hydromagnetic Dynamo Models. *Astrophysical Journal*, 122:293, 1955.

W. H. Press. *Numerical recipes in FORTRAN: the art of scientific computing*. 1992.

E. R Priest. *Solar Magnetohydrodnamics*. 1982.

M. Stix. Differential rotation and the solar dynamo. *Astronomy and Astrophysics*, 47(3):243, 1976.

M. Stix. *The Sun : an introduction*. 2004.

S. M. Tobias. Grand minima in nonlinear dynamos. *A&A*, 307:L21, 1996.

S. M. Tobias. The solar cycle: parity interactions and amplitude modulation. *A&A*, 322:1007, 1997.

S. M. Tobias. The solar dynamo. *Royal Society of London Philosophical Transactions Series A*, 360:2741, 2002.